PCCP

Synthesis and Photophysics of Gold(I) Alkynyls Bearing a Benzothiazole-2,7-Fluorenyl Moiety: A Comparative Study Analyzing Influence of Ancillary Ligand, Bridging Moiety, and Number of Metal Centers on Photophysical Properties

Journal:	*Physical Chemistry Chemical Physics*
Manuscript ID	CP-ART-03-2020-001539.R1
Article Type:	Paper
Date Submitted by the Author:	28-Apr-2020
Complete List of Authors:	Mihaly, Joseph J; Case Western Reserve University Phillips, Alexis; Air Force Research Laboratory Materials and Manufacturing Directorate Stewart, David; Air Force Research Laboratory Materials and Manufacturing Directorate, Marsh, Zachary; Air Force Research Laboratory Materials and Manufacturing Directorate, RXAP McCleese, Christopher; Case Western Reserve University, Haley, Joy; Air Force Research, Laboratory, Materials and Manufacturing Directorate Zeller, Matthias; Youngstown State University, Department of Chemistry Grusenmeyer, Tod; Air Force Research Laboratory Materials and Manufacturing Directorate, RXAP Gray, Thomas; Case Western Reserve University, Department of Chemistry

Synthesis and Photophysics of Gold(I) Alkynyls Bearing a Benzothiazole-2,7-Fluorenyl Moiety: A Comparative Study Analyzing Influence of Ancillary Ligand, Bridging Moiety, and Number of Metal Centers on Photophysical Properties

Joseph J. Mihaly,[a‡] Alexis T. Phillips,[b,e‡] David J. Stewart,[b,c] Zachary M. Marsh,[b,d] Christopher L. McCleese,[b,c] Joy E. Haley,[b] Matthias Zeller,[f] Tod A. Grusenmeyer,[b] and Thomas G. Gray[a,*]

[a]Department of Chemistry, Case Western Reserve University, 10900 Euclid Avenue, Cleveland, Ohio 44106, United States

[b]Air Force Research Laboratory, Materials and Manufacturing Directorate, Wright-Patterson Air Force Base, Dayton, Ohio 45433, United States

[c]General Dynamics Information Technology, 5000 Springfield Pike, Dayton, Ohio, 45431, United States

[d]Azimuth Corporation, 4027 Colonel Glenn Hwy. Suite 230, Beavercreek, OH United States 45431

[e]Southwestern Ohio Council for Higher Education, Dayton, Ohio, 45420, United States

[f]Department of Chemistry, Purdue University, West Lafayette Indiana, 47907, United States

Abstract: Three new gold(I) alkynyl complexes **(Au-ABTF(0-2))** containing a benzothiazole fluorenyl moiety, with either an organic phosphine or *N*-heterocyclic carbene as ancillary ligand, have been synthesized and photophysically characterized. All three complexes display highly structured ground-state absorption and luminescence spectra. Dual-luminescence is observed in all three complexes at room temperature in toluene after three freeze-pump-thaw cycles. The phosphine complexes **(Au-ABTF(0-1))** exhibit similar photophysics with fluorescent quantum yields ~0.40, triplet-state quantum yields ~0.50, and fluorescent lifetimes ~300 ps. The carbene complex **Au-ABTF2** displays different behavior; having a fluorescent quantum yield of 0.23, a triplet-state quantum yield of 0.61, and a fluorescent lifetime near 200 ps, demonstrating that the ancillary ligand alters excited-state dynamics. The compounds exhibit strong (on the order of 10^5 M^{-1} cm^{-1}) and positive excited-state absorption in both their singlet and triplet excited states spanning the visible region. Delayed fluorescence resulting from triplet-triplet annihilation is also observed in freeze-pump-thaw deaerated samples of all the complexes in toluene. DFT calculations (both static and time-resolved) agree with the photophysical data where phosphine complexes have slightly larger S_1 -T_2 energy gaps (0.28 eV and 0.26 eV) relative to the carbene complex (0.21 eV). Comparison of the photophysical properties of **Au-ABTF(0-2)** to previously published dinuclear gold(I) complexes and mononuclear gold(I) aryl complexes bearing the same benzothiazole-2,7-fluorenyl moiety are made. Structure-property relationships regarding ancillary ligand, bridging moiety, and number of metal centers are drawn.

Introduction:

Cyclometalates of iridium(III), platinum(II), and (less so) gold(III) have wide use in organic light-emitting diodes (OLEDs),[1-15] light-emitting electrochemical cells,[16–19] nonlinear optical materials,[20-28] and bioimaging agents.[33–37] Their triplet-state photoreactivity supports applications in photoredox sensitization schemes,[38–44] and increasingly in photodynamic therapy.[45–50] Much progress has resulted from fundamental investigations of cyclometalated iridium(III) and platinum(II) complexes. In these species, the metal ion is chelated to conjugated aromatic ligands, leading to emissive triplet states having mixed ligand-centred (LC) and metal-to-ligand charge transfer character (MLCT). The organic ligands are readily modified by synthesis, and a range of excited states with variable metal and ligand character are accessible. When the heavy atom contributes to frontier orbitals, spin-orbit coupling is efficient, and phosphorescence can often be observed.

Gold(I), with its closed $5d^{10}$ valance shell, is less apt to engage in d-π^* back bonding, yet many gold(I) complexes are phosphorescent, often with microsecond-scale radiative lifetimes.[51-63] The spin-orbit coupling parameter (ζ_I) of gold is the highest within the d-block transition metals.[80] Due to the observation of phosphorescence in many gold(I) complexes, the magnitude of ζ_I likely compensates for the lack of metal-to-ligand charge transfer character in these chromophores. A practical outcome of this filled 5d shell is that gold(I) organometallics can be more linearly transparent to visible light than platinum(II) analogues.[25,26,30–32] Che and co-workers have recently discussed the importance of attachment site when chromophores are metalated by σ-bonds to gold.[64,65] Spin-orbit coupling within the ligand is enhanced when gold is bound at carbon sites having high frontier orbital density. Similar observations have been made in transient absorption studies of gold(I) substituted pyrenyls.[66] We have demonstrated that binding of a single gold atom

to an aryl, triazolyl, or alkynyl carbon atom can afford dual fluorescence and phosphorescence emission.[66–69] Recent work has produced single-component white-light emitters through the combination of fluorescence and phosphorescence in equal quantum yields; these white-emitting compounds are (organophosphine)gold(I) aryls, where the aryl group is the benzothiazole fluorenyl (BTF) conjugate seen in the left panel of Figure 1.[70]

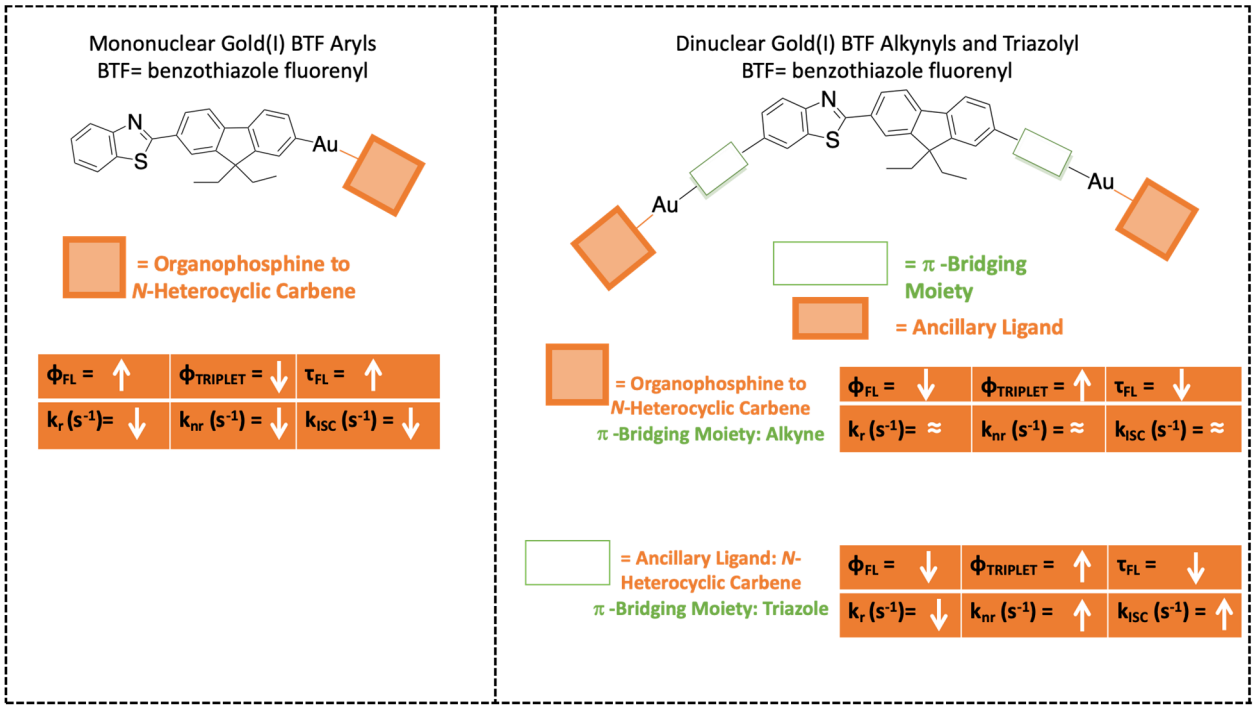

Figure 1. Summary of previous gold(I) work demonstrating structure-property relationships in gold(I) complexes of the fluorenyl-benzothiazolyl (BTF) moiety.

Photophysical analysis of gold(I) BTF aryl compounds (Figure 1, left) finds that choice of ancillary ligand has a marked effect on the excited-state dynamics. As the ancillary ligand is changed from organophosphine (**Au-BTF(0-1)**) to *N*-heterocyclic carbene (**Au-BTF2**), the rate of intersystem crossing is diminished along with a decrease in both the radiative and non-radiative decay rates. This corresponds with an enhancement in the fluorescence lifetime, fluorescence quantum yield, and diminished intersystem crossing efficiency in **Au-BTF2**.[70] In subsequent work, dinuclear

gold(I) alkynyls (**Au-DiBTF(0-2)**) and a triazolyl (**Au-DiBTF3**) were photophysically analyzed (Figure 1, right).[71] Addition of two gold atoms does not increase k_{isc} or the intersystem crossing efficiency relative to the mononuclear gold(I) aryl compounds. Interestingly, changing the ancillary ligand in the dinuclear gold(I) BTF alkynyls from an organophosphine (**Au-DiBTF(0-1)**) to an *N*-heterocyclic carbene (**Au-DiBTF(2)**) results in only incremental fluctuations in the intersystem crossing efficiency, fluorescence quantum yield, and fluorescence lifetime. The rate constants of radiative and non-radiative decay as well as intersystem crossing are nearly identical in the dinuclear gold(I) BTF alkynyls (**Au-DiBTF(0-2)**). Changing the alkynyl bridge to a triazolyl in the carbene complex (**Au-DiBTF3**) leads to appreciably different excited-state dynamics; an increase in intersystem crossing efficiency is observed along with a decrease in fluorescence quantum yield and fluorescence lifetime. These variations in excited-state behavior are due to an increase in the rate of intersystem crossing and non-radiative decay with a decrease in the rate of radiative decay. In light of these results, we have synthesized and photophysically characterized the analogous mononuclear gold(I) BTF alkynyl complexes. The gold(I) alkynyl complexes **(Au-ABTF(0-2))** contain a benzothiazole fluorenyl moiety, with either an organic phosphine or *N*-heterocyclic carbene as ancillary ligand. The effects of the ancillary ligand (organophosphine or *N*-heterocyclic carbene) as well as the nature of the linkage between the gold atom and organic chromophore on the photophysical properties in these chromophores elicits continuing interest. This work serves to present the photophysical properties of the newly synthesized Au-ABTF chromophores as well as to compare the photophysical properties of the aryl, alkynyl, and dinuclear gold(I) chromophores in the series. This exploration of the structure-property relationships provides for the discussion of the rational design of triplet-active organogold(I) chromophores.

Results and Discussion

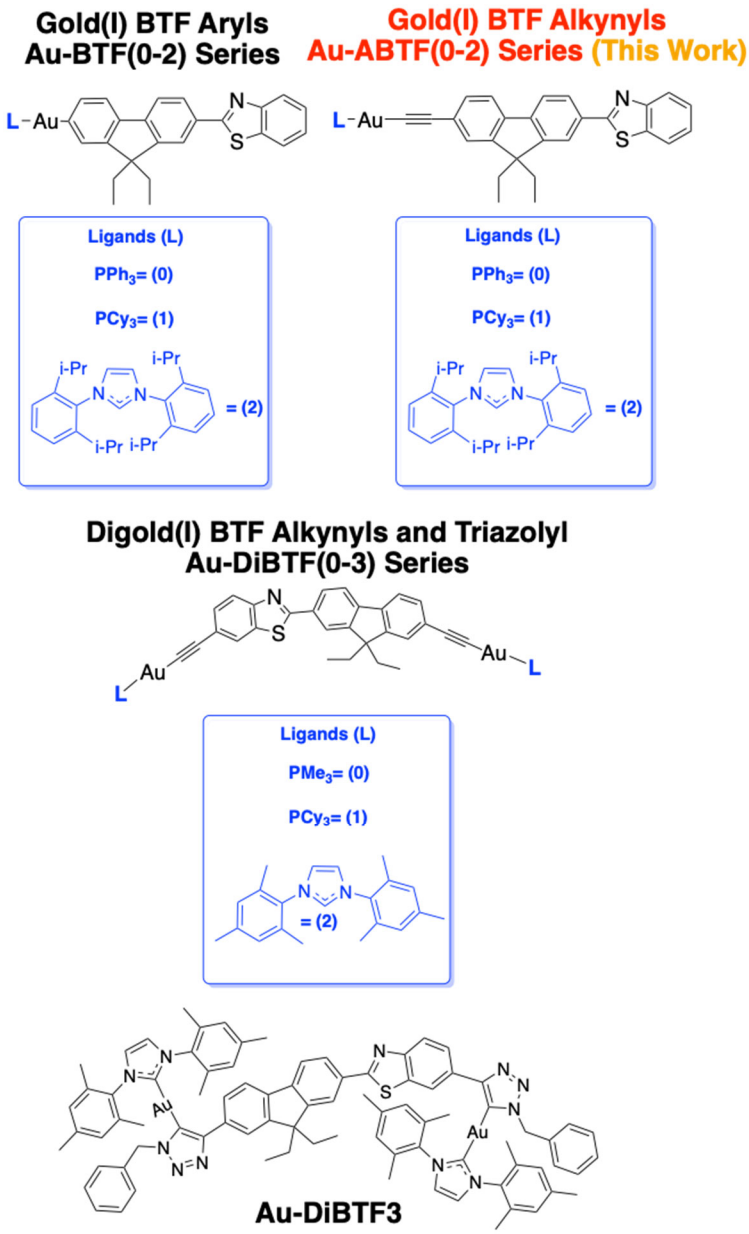

Figure 2. Designation of gold(I) benzothiazole-fluorenyl chromophores.

Reaction of the known benzothiazole-2,7-fluorenyl alkyne[72] with (phosphine-) or (*N*-heterocyclic carbene)gold(I) chlorides[67–69,73] at room temperature afforded the corresponding (alkynyl)gold(I) species **Au-ABTF0** (79% yield), **Au-ABTF1** (60% yield), and **Au-ABTF2** (76% yield), Scheme 1. Diffraction quality crystals were grown from vapor diffusion of pentanes into concentrated dichloromethane solutions. A thermal ellipsoid depiction of **Au-ABTF1** appears in Figure 3.

Crystal structures of **Au-ABTF0** and **Au-ABTF2** appear in the supporting information (Figures S8 and S2, respectively). Geometric parameters are unexceptional, and all complexes are two-coordinate and essentially linear. Aurophilic interactions and π-stacking are not observed in the packing diagrams for any of the compounds.

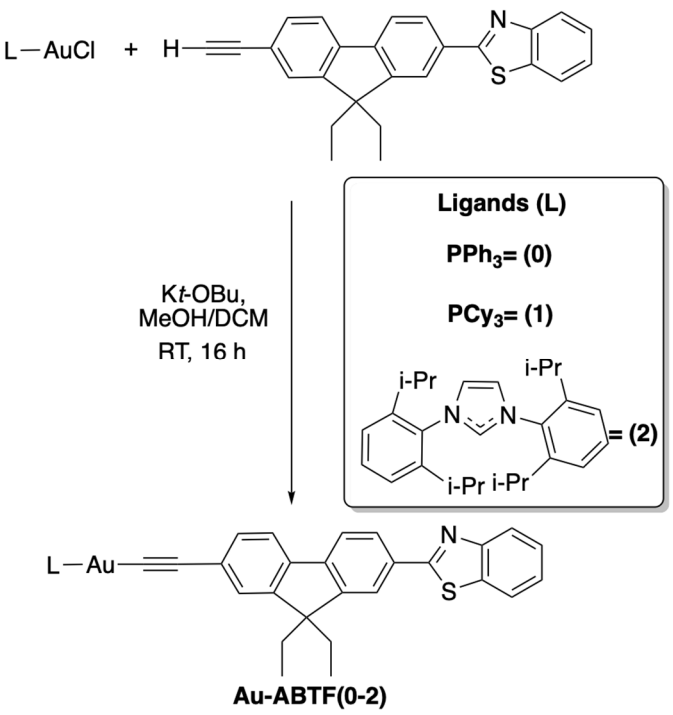

Scheme 1. Synthesis of **Au-ABTF(0-2)**.

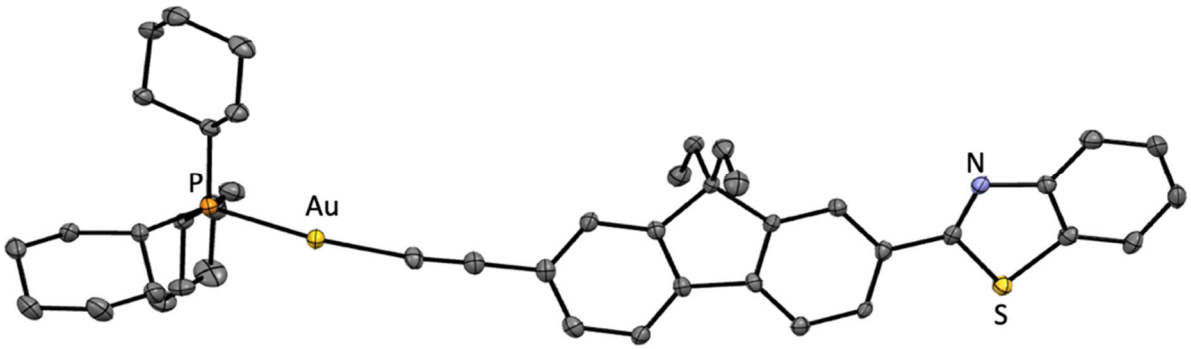

Figure 3. Thermal ellipsoid representation of **Au-BTF1** (50% probability level, 150 K). Hydrogen atoms are omitted for clarity. Unlabeled atoms are carbon.

Thermogravimetric analysis in air was also performed on the compounds in order to assess their thermal stabilities. Plots of weight loss as a function of temperature appear in Figure S1 (Supporting Information). The onset of weight loss is observed at ~230 °C in both **Au-ABTF0** and **Au-ABTF1** and 345° C in **Au-ABTF2**.

Ground-state absorption and steady-state luminescence spectroscopy. Ground-state absorption spectra and steady-state luminescence spectra in toluene following three freeze-pump-thaw cycles appear in Figure 4. Ground-state absorption, luminescence wavelength maxima, singlet and triplet excited-state energies, and ground-state extinction coefficient values are reported in Table 1. Data collected for the previously reported gold(I) compounds is included for comparison.

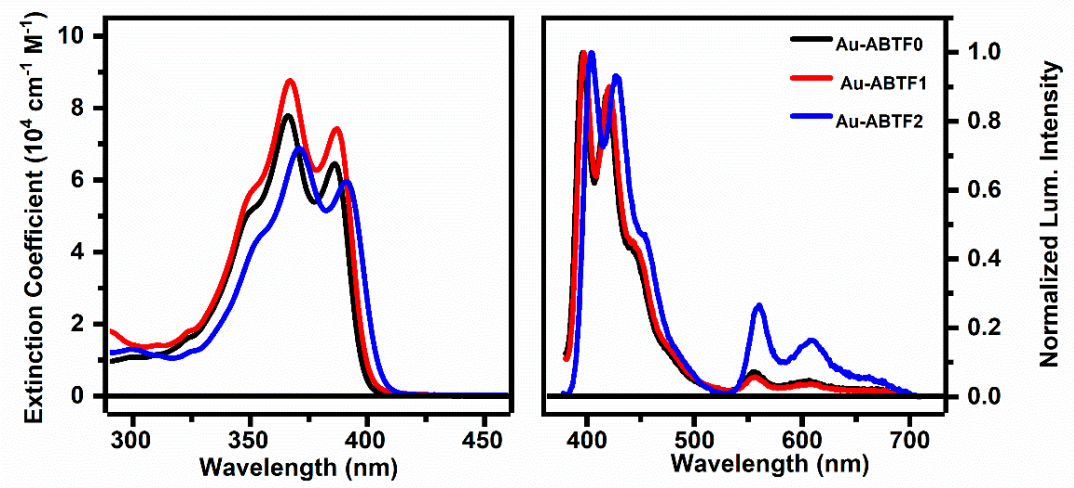

Figure 4. Absorption (left) and luminescence (right) spectra of **Au-ABTF0** (black), **Au-ABTF1** (red), and **Au-ABTF2** (blue). The emission spectra were collected in toluene at room temperature following three freeze-pump-thaw degas cycles.

(Phosphine)gold(I) complexes **Au-ABTF0** and **Au-ABTF1** have similar ground-state absorption spectra with peak maxima occurring at 366 nm and 367 nm, respectively. Changing the ancillary ligand to an *N*-heterocyclic carbene in **Au-ABTF2** results in a bathochromic shift of the absorption

maxima to 371 nm. The band shapes of the ground-state absorption spectra are similar and structured in all three complexes. The ground-state extinction coefficients for these compounds range from 6 - 9 x 10^4 M^{-1} cm^{-1}. The ground-state absorption spectra of **Au-ABTF(0-2)** are similar in band shape and extinction coefficient to the free alkyne; however, the gold(I) ABTF complexes (**Au-ABTF(0-2))** display a bathochromic shift relative to the parent alkyne, which has a ground-state absorption maximum of 351 nm in benzene.[74]

Table 1. Pertinent ground-state absorption and steady-state luminescence data.

	Au Complex	Experimental Results					
		λ_{ABS}/nm (10^4 $M^{-1}cm^{-1}$)	λ_{FL}[B] (nm)	E_S[C] (eV)	λ_{PHOS}[B] (nm)	E_T[C] (eV)	ΔE_{ST} (eV)
Alkynyl	**Au-ABTF0**	366 (7.79)	396	3.13	555	2.23	0.90
	Au-ABTF1	367 (8.77)	397	3.12	556	2.23	0.89
	Au-ABTF2	371 (6.89)	404	3.07	560	2.21	0.86
Aryl	**Au-BTF0**	359 (5.34)	388	3.20	538	2.30	0.90
	Au-BTF1	360 (5.95)	389	3.19	538	2.30	0.89
	Au-BTF2	364 (5.80)	397	3.12	541	2.29	0.83
Dinuclear	**Au-DiBTF0**	383 (6.00)[A]	413	3.00	575	2.16	0.84
	Au-DiBTF1	384 (5.10)[A]	413	3.00	575	2.16	0.84
	Au-DiBTF2	387 (6.76)[A]	418	2.97	580	2.14	0.83
	Au-DiBTF3	390 (6.99)[A]	427	2.90	570	2.18	0.72

Data collected in toluene unless otherwise noted.
[A]Collected in dichloromethane due to limited solubility in toluene.
[B]Estimated from the luminescence maximum.
[C]Estimated value of the luminescence maximum first converted to wavenumbers and then to values in eV.

These results are consistent with BTF-localized π-π^* absorption transitions in all three **Au-ABTF(0-2)** complexes. These findings agree with previously published results on the **Au-BTF(0-2)** and **Au-DiBTF(0-3)** complexes; these complexes also possess highly structured ground-state

absorption spectra attributed to π-π^* absorption transitions localized on the BTF ligand. The nature of the bridging ligand, the ancillary ligand, and the number of gold(I) metal centers influences the energy of the ground-state absorption transitions in this series of complexes. The gold(I) BTF aryl complexes (**Au-BTF(0-2)**) absorb at shorter wavelengths than their alkynyl counterparts (**Au-ABTF(0-2)**) with similar ancillary ligand effects. (Phosphine)gold(I) aryls **Au-BTF0** and **Au-BTF1** possess absorption maxima at 359 nm and 360 nm, respectively, and the (carbene)gold(I) complex **Au-BTF2** shows an absorption maximum at 364 nm. On the other hand, dinuclear gold(I) complexes, **Au-DiBTF(0-3)**, exhibit ground-state absorption maxima at wavelengths longer than those of mono-alkynyl gold(I) BTF (**Au-BTF(0-2)**) complexes. When the dinuclear gold(I) species possesses a phosphine ancillary ligand, the ground-state absorption maximum occurs at 383 nm in **Au-DiBTF0** and 384 nm in **Au-DiBTF1**. Inclusion of the *N*-heterocyclic carbene ancillary ligand shifts the ground-state absorption maxima to 387 nm in **Au-DiBTF2**. A further bathochromic shift occurs when the alkynyl bridging moiety in **Au-DiBTF2** is converted to a triazole linkage; the ground-state absorption maximum of **Au-DiBTF3** occurs at 390 nm. The monogold(I) alkynyls (**Au-ABTF(0-2))** all exhibit dual luminescence in freeze-pump-thaw deaerated toluene. The observed fluorescence is much more intense than the phosphorescence in these complexes. The fluorescence and phosphorescence maxima parallel the ground-state absorption maxima with **Au-ABTF0** $\approx$ **Au-ABTF1** $>$ **Au-ABTF2**. The fluorescence and phosphorescence are highly structured, and appear as a mirror image of the ground-state absorption spectra. This observation implies that the luminescence from these complexes is also π-π^* in nature. The aryl complexes (**Au-BTF(0-2)**) and dinuclear gold(I) BTF complexes (**Au-DiBTF(0-3))** also demonstrate structured luminescence and follow the same excited-state energy trends. Structural variation has the greatest influence on the relative intensity of the fluorescence and phosphorescence in the

steady-state luminescence spectra of these complexes. The intensity of the fluorescence and phosphorescence in the aryl gold(I) complexes (**Au-BTF(0-2)**) is similar in the phosphine containing complexes, **Au-BTF0** and **Au-BTF1**, resulting in white light emission. The fluorescence intensity is enhanced relative to the phosphorescence when a *N*-heterocyclic carbene ancillary ligand is utilized in **Au-BTF2**. The steady-state emission from this complex appears violet. The observed phosphorescence in the laterally asymmetric dinuclear gold(I) complexes (**Au-DiBTF(0-3)**) is extremely weak in comparison to monogold aryl or alkynyl BTF complexes. This echoes earlier observations that spin-orbit coupling is hindered in dinuclear gold(I) species when gold(I) centers are widely separated.[26,74–78] The phosphorescence signal is strong enough in (**Au-ABTF(0-2))** and (**Au-BTF(0-2)**) for us to measure the phosphorescence lifetimes of the complexes. All of the molecules have phosphorescence lifetimes of greater than 500 μs. The observation of both fluorescence and phosphorescence in the alkynyl (**Au-ABTF(0-2))**, aryl (**Au-BTF(0-2)**), and dinuclear BTF (**Au-DiBTF(0-3)**) complexes allows for a comparison of the singlet-triplet energy gaps (ΔE_{ST}**)** in these molecules. In the mononuclear gold(I) molecules, the magnitude of the singlet-triplet energy gap is essentially identical when a phosphine is present as the ancillary ligand. Interestingly, the magnitude of the singlet-triplet gap is quantitatively smaller in the mononuclear gold complexes when a *N*-heterocyclic carbene is used as the ancillary ligand. The singlet-triplet energy gap is generally smaller in the dinuclear gold(I) molecules. The singlet-triplet gaps in the dinuclear compound are less sensitive to changes in the ancillary ligands (phosphine to *N*-heterocyclic carbene) but are greatly influenced by the nature of the bridging moiety (alkyne to triazole). Changing the bridging moiety from an alkynyl moiety (**Au-DiBTF2**) to a triazole (**Au-DiBTF3**) results in a greater than 100 meV change in the singlet-triplet gap.

Fluorescence quantum yields, intersystem crossing quantum yields, and luminescence lifetimes. Fluorescence and phosphorescence lifetimes (Figure S10), fluorescence quantum yields (Figure S11), phosphorescence quantum yields (Figure S12), and intersystem crossing quantum yields (Figure S13) results for the alkynyl gold(I) complexes are summarized in Table 2. The values obtained for previously studied gold(I) complexes are again included for comparison. **Au-ABTF0** and **Au-ABTF1** display similar excited-state properties. Both complexes have fluorescence quantum yield values of approximately 0.40, intersystem crossing quantum yield values near 0.50, and fluorescence lifetimes of roughly 300 ps. **Au-ABTF2** features a diminished fluorescence quantum yield value 0.23, an enhanced intersystem crossing quantum yield value of 0.61, and a shorter fluorescence lifetime of about 200 ps. Combined, the fluorescence quantum yield, intersystem crossing quantum yield, and fluorescence lifetime values allow for the calculation of the radiative (k_r), non-radiative (k_{nr}), and intersystem crossing (k_{ISC}) rate constants in these complexes (See SI). The calculated values for k_r are similar for (**Au-ABTF(0-2)**) with all of the values on the order of 1.0 x 10^9 s^{-1}. The magnitude of k_{isc} is two times larger in the *N*-heterocyclic carbene complex **Au-ABTF2,** relative to the phosphine containing derivatives, **Au-ABTF0** and **Au-ABTF1**. The value of k_{isc} was determined to be 3.0 x 10^9 s^{-1} for **Au-ABTF2** compared with values of 1.5 x 10^9 s^{-1} and 1.6 x 10^9 s^{-1} for **Au-ABTF0** and **Au-ABTF1**, respectively. Non-radiative decay is found to be a minor contributor to the excited-state dynamics in all of the Au-ABTF derivatives. The values of k_{nr} are all $\leq$ 0.78 x 10^9 s^{-1}.

Table 2. Pertinent Quantum Yield and Lifetime Data.

	Au Complex	Experimental Results							
		φ_{FL}	τ_{FL}[A] (ps)	k_r[B] (10^9 s^{-1})	k_{nr}[B] (10^9 s^{-1})	k_{ISC}[B] (10^9 s^{-1})	$\varphi_{TRIPLET}$	φ_{PHOS}	τ_{PHOS} (μs)
Alkynyl	**Au-ABTF0**	0.41 ± 0.03	308 ± 6	1.3	0.39	1.5	0.47 ± 0.04	0.02 ± 0.01	715 ± 200
	Au-ABTF1	0.44 ± 0.01	338 ± 2	1.3	0.10	1.6	0.53 ± 0.01	0.06 ± 0.01	492 ± 100
	Au-ABTF2	0.23 ± 0.02	206 ± 13	1.1	0.78	3.0	0.61 ± 0.02	0.04 ± 0.01	609 ± 50
Aryl	**Au-BTF0**	0.08 ± 0.01	79.3	0.94	1.5	9.3	0.79 ± 0.01	0.09 ± 0.01	810 ± 70
	Au-BTF1	0.09 ± 0.03	89.4	0.95	1.1	8.5	0.81 ± 0.02	0.07 ± 0.01	766 ± 8
	Au-BTF2	0.22 ± 0.01	229	0.80	0.54	2.3	0.63 ± 0.03	0.11 ± 0.01	872 ± 59
Dinuclear	**Au-DiBTF0**	0.55 ± 0.02	438 ± 5	1.3	≤ 0.02	1.2	0.51 ± 0.02	---[C]	---[C]
	Au-DiBTF1	0.55 ± 0.02	442 ± 1	1.2	≤ 0.05	0.97	0.43 ± 0.02	---[C]	---[C]
	Au-DiBTF2	0.44 ± 0.01	380 ± 1	1.2	≤ 0.03	1.5	0.57 ± 0.02	---[C]	---[C]
	Au-DiBTF3	0.28 ± 0.02	369 ± 1	0.76	0.11	2.4	0.68 ± 0.01	---[C]	---[C]

All values collected in toluene.
[A]Values determined using time-correlated single photon counting.
[B]System of equations used for the rate constant determinations are shown in the SI.
[C]Phosphorescence lifetime and quantum yield values were not determined due to weak signal.

The magnitude of k_r is similar for all of the alkynyl (**Au-ABTF(0-2)**), aryl (**Au-BTF(0-2)**), and dinuclear BTF (**Au-DiBTF(0-3)**) complexes; the calculated values of k_r across the series of molecules are all within a factor of two. The excited-state dynamics in these molecules are largely controlled by variations in the values of k_{nr} and k_{ISC}. For the mononuclear aryl complexes with phosphine ancillary ligands (**Au-BTF(0-1)**), the magnitude of k_{nr} and k_{ISC} are the largest in the series. This results in molecules with low fluorescence quantum yields and high intersystem crossing quantum yields. Changing the ancillary ligand to a *N*-heterocyclic carbene in **Au-BTF2** diminishes the values of k_{nr} and k_{ISC}, resulting in an increase in the fluorescence quantum yield and a decrease in the intersystem crossing quantum yield. The dinuclear BTF (**Au-DiBTF(0-3)**) complexes generally have the smallest values of k_{nr} in the series. When the alkynyl bridge is

present in these molecules, regardless of ancillary ligand, k_{nr} is an order of magnitude lower than all of the other complexes. Although two gold(I) atoms are present, the rate of intersystem crossing is similar to that of the mononuclear alkynyl compounds. This is consistent with previously reported dinuclear gold(I) chromphores.[26,74–78] The magnitude of the fluorescence quantum yield and intersystem crossing quantum yield are similar in the alkynyl bridged, dinuclear species (**Au-DiBTF(0-2)**). **Au-DiBTF3** contains a triazole linkage and a *N*-heterocyclic carbene ancillary ligand. This molecule has the smallest value of k_r in the series and a value of k_{ISC} that is two times larger than the other dinuclear compounds. **Au-DiBTF3** has the largest intersystem crossing quantum yield and lowest fluorescence quantum yield of the dinuclear complexes.

Nanosecond transient absorption and delayed fluorescence. Nanosecond transient absorption spectra in units of Δε vs. wavelength for **Au-ABTF (0-2)** collected in freeze-pump-thaw deaerated toluene are displayed in Figure 5. Excited-state extinction coefficients at the maximum of the T_1-T_n transition and triplet-triplet annihilation fit parameters are given in Table 3. The values obtained for the structurally similar gold(I) aryl compounds are included in Table 3 for comparison. All of the compounds are characterized by a bleach of the ground-state absorption spectrum and strong, positive excited-state absorption from 400 nm to 750 nm. Energy trends coincide with the ground-state absorption data; namely, a slight bathochromic shift in the triplet-triplet absorption maximum ($\boldsymbol{\lambda_T}$) is observed when the ancillary ligand is varied from a phosphine (**Au-ABTF(0-1)**) to a *N*-heterocyclic carbene (**Au-ABTF2**). The triplet-triplet absorption in these complexes is strong. Relative actinometry experiments with $[Ru(bpy)_3]^{2+}$ were performed in order to determine the triplet excited state extinction coefficients for **Au-ABTF(0-2)**. The magnitude of the excited-state extinction coefficient ($\boldsymbol{\Delta\varepsilon_{T_1-T_n}}$) for all of the molecules is on the order of 10.0 x 10^4 M^{-1} cm^{-1}.

Table 3. Pertinent Transient Absorption and Triplet-Triplet Annihilation Data.

	Au Complex		Experimental Results			
		$\Delta\varepsilon_{S_1-S_n}/\lambda$ nm[A] (10^4 M^{-1} cm^{-1})	τ_{TA}[C] (ps)	$\Delta\varepsilon_{T_1-T_n}/\lambda$ nm[A] (10^4 M^{-1} cm^{-1})	k_T[B] (s^{-1})	k_{TT}[B] (M^{-1} s^{-1})
Alkynyl	Au-ABTF0	620 (21.1)	288 ± 7	592 (14.0 ± 2.0)	3,000	$9.2 \pm 0.3 \times 10^9$
	Au-ABTF1	634 (36.5)	301 ± 7	595 (13.8 ± 3.0)	2,030	$1.4 \pm 0.2 \times 10^{10}$
	Au-ABTF2	624 (18.9)	192 ± 4	610 (9.0 ± 4.0)	1,630	$2.5 \pm 0.7 \times 10^{10}$
Aryl	Au-BTF0	565 (13.7)	84.5 ± 4.6	545 (9.14 ± 0.50)	1,220	$1.3 \pm 0.1 \times 10^{10}$
	Au-BTF1	588 (15.6)	95.4 ± 2.3	551 (10.1 ± 0.10)	1,290	$1.2 \pm 0.1 \times 10^{10}$
	Au-BTF2	558 (15.0)	279 ± 10	565 (9.40 ± 0.10)	1,140	$1.4 \pm 0.1 \times 10^{10}$

All values collected in toluene.
[A]Methodology used to determine excited-state extinction coefficients is discussed in the SI.
[B]Methodology used to determine values of k_T and k_{TT} is discussed in the SI.
[C]Average values obtained from a global lifetime analysis completed at 10 unique wavelengths.

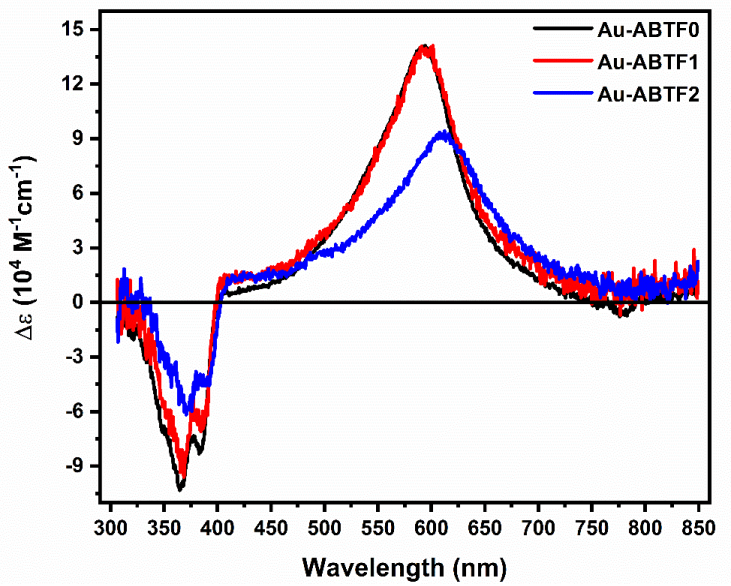

Figure 5. Nanosecond transient absorption spectra of **Au-ABTF0** (black), **Au-ABTF1** (red), and **Au-ABTF2** (blue). All samples were excited at 355 nm and collected 100 ns after the laser pulse. Relative actinometry experiments allowed for conversion to units of Δε.

Nanosecond transient absorption kinetic decay traces were collected at the triplet-triplet absorption maximum (λ_T) of each molecule. The kinetic decay traces collected at two laser energies for **Au-**

ABTF0 are shown in Figure 6 (right). Plots showing the kinetic decay traces for **Au-ABTF1** and **Au-ABTF2** are shown in Figure S16. Two laser energies were used to obtain kinetic traces in order to investigate the effect of the excitation pulse energy on the decay of the triplet excited-state. An increase in the laser pulse energy leads to an increase in the triplet excited-state concentration and coincides with an increase in the initial rate of excited-state decay. This, in combination with observable delayed fluorescence, indicates that triplet-triplet annihilation occurs in all three gold(I) alkynyl complexes. The delayed fluorescence signal was observed as a function of laser pulse energy. Figure 6 (left) shows the normalized integrated delayed fluorescence vs. the incident laser energy with the best quadratic fit for **Au-ABTF0**; plots for **Au-ABTF1** and **Au-ABTF2** appear in Figure S14. The inset in Figure 6 (left) shows the double logarithm plot with the corresponding linear fit. The slope of the double logarithm plot for all complexes is nearly 2, indicating a bimolecular process leads to the observed delayed fluorescence.[79] Figure 6 (right) shows the kinetic decay traces obtained in our nanosecond transient absorption measurements in units of concentration vs time. The raw ΔOD vs time spectra were converted into units of concentration vs time using the previously determined triplet excited-state extinction coefficients. This data conversion allows for the determination of the rate constants of triplet-triplet annihilation (k_{TT}).[79] The collection of phosphorescence lifetimes for these molecules allowed us to determine values for the rate constant governing the intrinsic decay of the triplet excited-state (k_T). The value of k_T was held constant in the triplet-triplet annihilation fits of the transient absorption decay traces obtained for all three **Au-ABTF** chromophores. The values of k_{TT} range from 9.2×10^9 M^{-1} s^{-1} in **Au-ABTF0** to 2.5×10^{10} M^{-1} s^{-1} in **Au-ABTF2**, signifying that triplet-triplet annihilation is a diffusion controlled process in toluene solutions containing **Au-ABTF(0-2)**.[80]

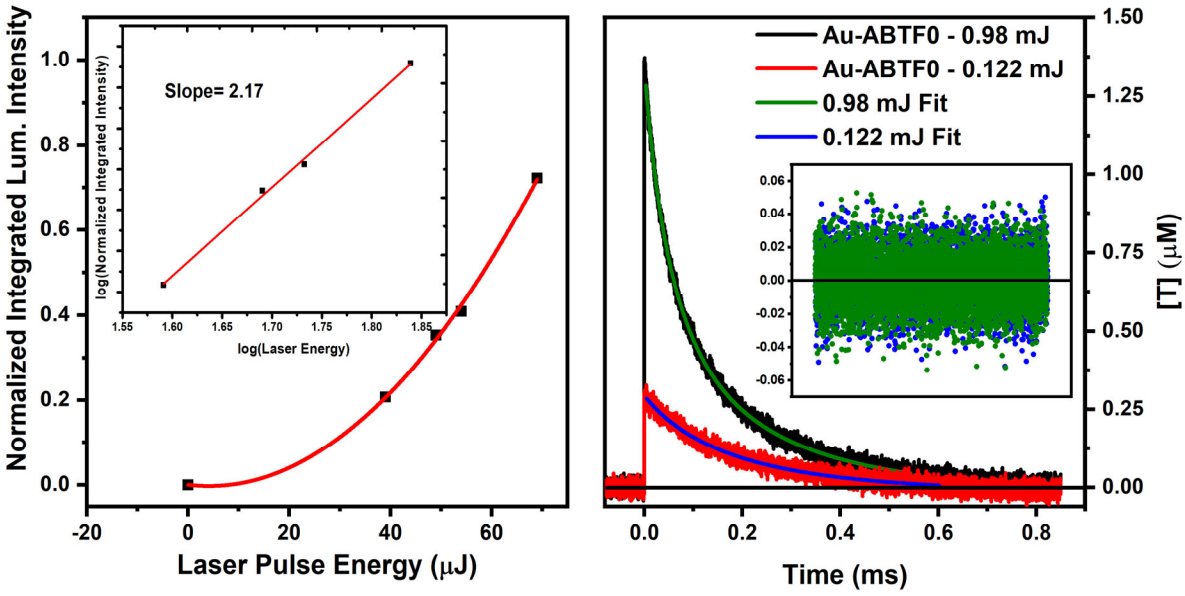

Figure 6. Au-ABTF0 Normalized integrated fluorescence intensity vs. laser pulse energy (left) and triplet-triplet annihilation fit of excited state decay (right). Both figures correspond to freeze-pump-thaw deaerated solutions in toluene. The left figure was fit to a quadratic and the left inset corresponds to the double logarithm plot fit linearly with a slope of 2.17. The right inset is the triplet-triplet annihilation fit residuals.

These nanosecond transient absorption results are similar to those obtained for the series of **Au-BTF** complexes. The nanosecond transient absorption spectra of **Au-BTF(0-2)** also exhibit a bleach corresponding to loss of ground-state absorption and broad, positive transient absorption throughout the visible region. The excited-state extinction coefficients of **Au-BTF(0-2)** are also on the order of 10.0 x 10^4 M^{-1} cm^{-1}. A red shift in the maximum of the triplet-triplet absorption spectrum is also observed in the **Au-BTF(0-2)** series when the phosphine ancillary ligand is swapped with the *N*-heterocyclic carbene ligand. The observation of strong, broad triplet-triplet absorption in **Au-ABTF(0-2)** and **Au-BTF(0-2)** is comparable to previous results obtained for Pt(II) alkynyl BTF complexes.[72] In general, the excited-state absorption spectra of **Au-BTF(0-2)** are broader than the excited-state absorption spectra of their **Au-ABTF(0-2)** counterparts. The maximum of the excited-state absorption feature is red-shifted in **Au-ABTF(0-2)** relative to **Au-BTF(0-2)**. Delayed fluorescence as a result of triplet-triplet annihilation is observed in both **Au-ABTF(0-2)** and **Au-BTF(0-2)**. Triplet-triplet annihilation is a diffusion limited process in both the

gold(I) aryl- and alkynyl-BTF complexes. Nanosecond transient absorption results were not described in our previous report on **Au-DiBTF(0-2)** due to much weaker triplet-triplet absorption in initial pulsed laser experiments on these molecules.[71]
The observation of strong excited-state absorption in **Au-ABTF(0-2), Au-BTF(0-2),** and previous reports on Pt(II) alkynyl BTFs but lack of strong excited-state absorption in **Au-DiBTF(0-2)** warrants further investigation.

Ultrafast Transient Absorption. Ultrafast transient absorption spectra for **Au-ABTF(0-2)** complexes in toluene are displayed in Figure 7. Excited-state extinction coefficients at the global maximum of the 0 picosecond trace and ultrafast transient absorption lifetime values are given in Table 3. The lifetime values displayed in Table 3 are average values obtained from a global lifetime analysis completed at 10 unique wavelengths. Previously obtained extinction coefficient and lifetime values are also included for gold(I) aryl compounds for comparison. Example monoexponential fits of a single kinetic decay trace collected for **Au-ABTF(0-2)** are shown in Figure S17. The transient absorption spectrum collected for each molecule is characterized by a broad, strong absorption feature. The maximum of the transient absorption signal occurs at 621 nm in **Au-ABTF0**, 635 nm in **Au-ABTF1**, and 625 nm in **Au-ABTF2**. As the absorption spectra evolve in time, the peak maximum of the absorption feature diminishes, leaving a transient absorption spectrum that strongly resembles the transient absorption spectrum obtained 100 ns after the laser pulse in nanosecond transient absorption experiments. The lifetime values obtained from ultrafast transient absorption measurements are in good agreement with the lifetime values obtained from TCSPC fluorescence lifetime measurements. An isosbestic point is also evident at ~510 nm in the spectra obtained for **Au-ABTF(0-2)**. This combination of factors indicates that the progression observed in the ultrafast transient absorption spectra from the 0 picosecond to 1000 picosecond time traces corresponds to evolution from the singlet excited-state to the triplet excited-state. The singlet excited-state extinction coefficient ($\boldsymbol{\Delta\varepsilon_{S_1-S_n}}$) values measured for all three molecules using the 0 ps transient absorption trace are extremely large; all are $\geq 18.9 \times 10^4$ M^{-1} cm^{-1}. In similar fashion to the nanosecond transient absorption results, the ultrafast transient absorption results obtained for **Au-ABTF(0-2)** also parallel the ultrafast transient absorption results obtained for **Au-BTF(0-2)**. The ultrafast transient absorption results on the **Au-BTF**

complexes also demonstrate a clear evolution from the singlet excited state to the triplet excited state, and the singlet excited-states in the **Au-BTF** complexes also possess large excited state extinction coefficients. The absorption maxima of the singlet excited state observed in the tricyclohexylphosphine containing complexes, **Au-BTF1** and **Au-ABTF1**, shows a bathochromic shift relative to the other chromophores in the series. Ultrafast transient absorption experiments were not performed on the **Au-DiBTF** series due to the lack of strong triplet-triplet absorption in those molecules. These experiments are ongoing.

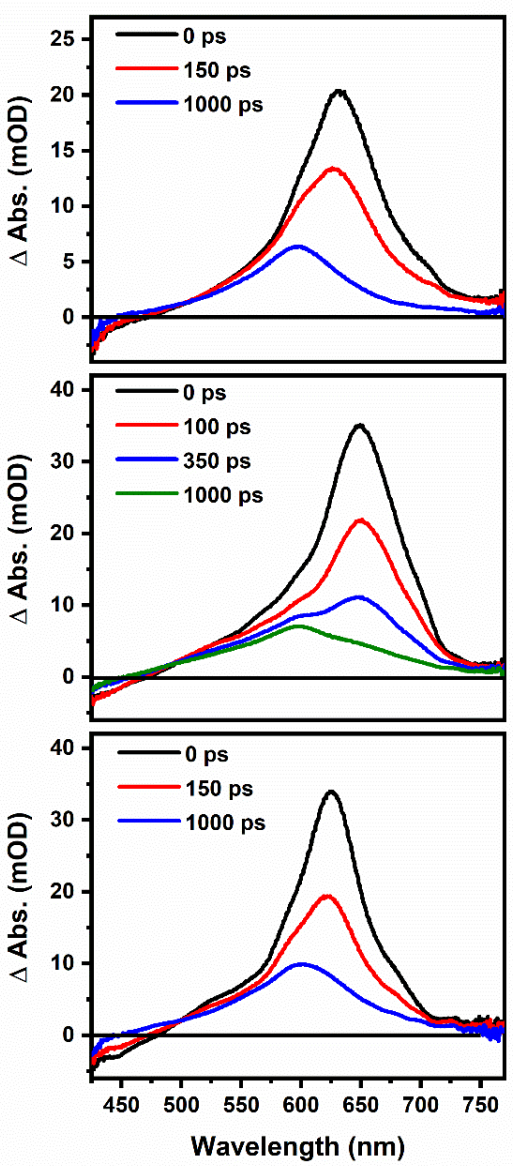

Figure 7. Ultrafast transient absorption spectra for **Au-ABTF0** (top), **Au-ABTF1** (middle), and **Au-ABTF2** (bottom) in toluene. All samples were excited at 400 nm using the frequency doubled output of a Ti:sapphire laser.

Calculations.

Density-functional theory calculations were performed in order to gain computational insight for the observed photophysics of **Au-ABTF(0-2)**. All geometries for the **Au-ABTF** compounds were optimized from the crystal structures. Figure 8 displays a frontier orbital energy level diagram and the corresponding frontier Kohn-Sham orbital plots for **Au-ABTF2**. Plots for **Au-ABTF0-1**

appear as Supporting Information, Figures S18 and S19. The highest occupied Kohn-Sham orbital (HOMO) and lowest unoccupied Kohn-Sham orbital (LUMO) derive almost entirely from the carbanionic alkynyl ligand in all complexes. The HOMO is comprised predominantly of the carbon-carbon triple bond (29% of electron density) and fluorenyl (56%) moiety with minor contributions from gold, the capping ligand, and the benzothiazolyl heterocycle. The LUMO shows a greater fraction of density on the benzothiazolyl moiety, with similar fluorenyl character. There is little density on the carbon-carbon triple bond and virtually none on gold. Natural transition orbitals calculated for the Franck-Condon S_1 and T_1 states of **Au-ABTF0-2** also indicate excited states centered on the alkynyl ligand (Figures S18–S22). These computations, combined with highly structured absorption and emission profiles suggest that the observable transitions derive from the alkynyl ligand.

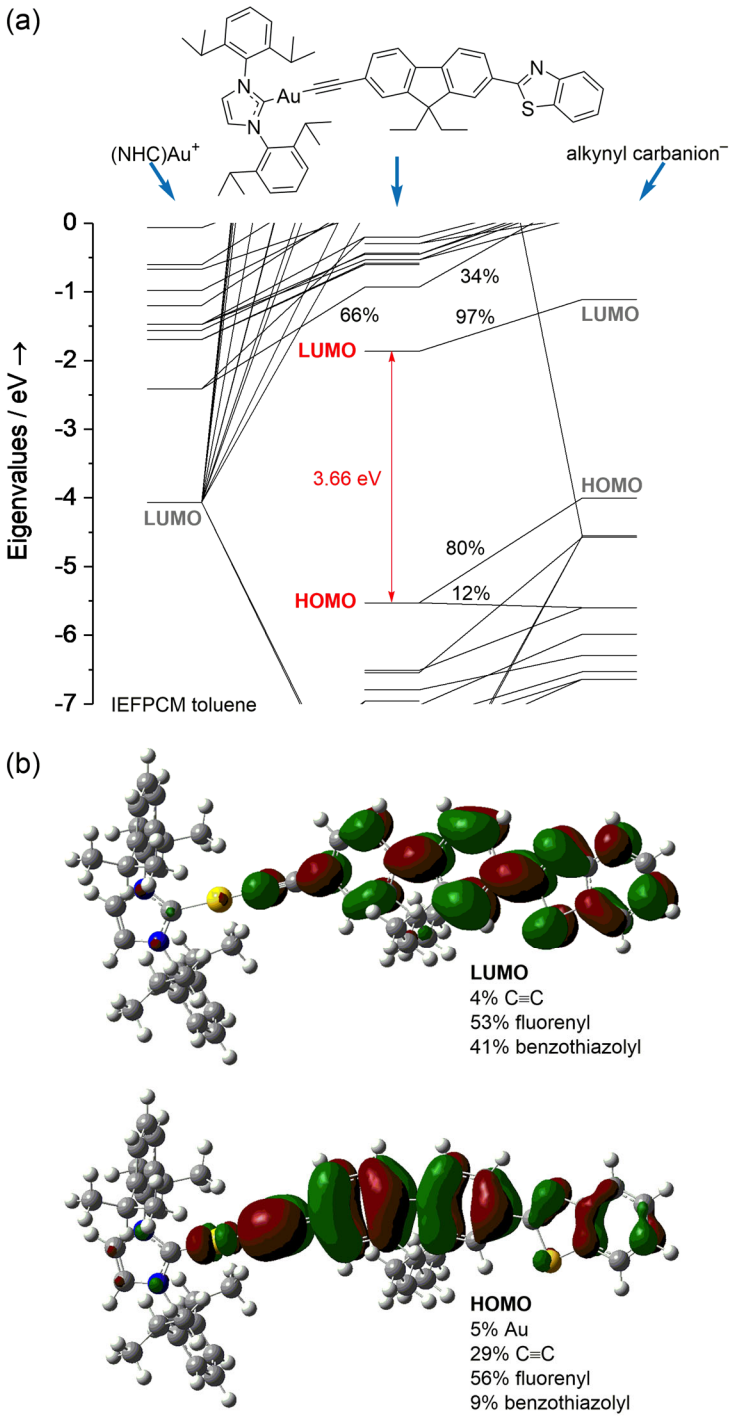

Figure 8. (a) Frontier orbital energy diagram of **Au-ABTF2**. (b) Kohn-Sham orbital plots (HOMO and LUMO) for **Au-ABTF2**. Percentages are of electron density; contour levels 0.02 a.u.

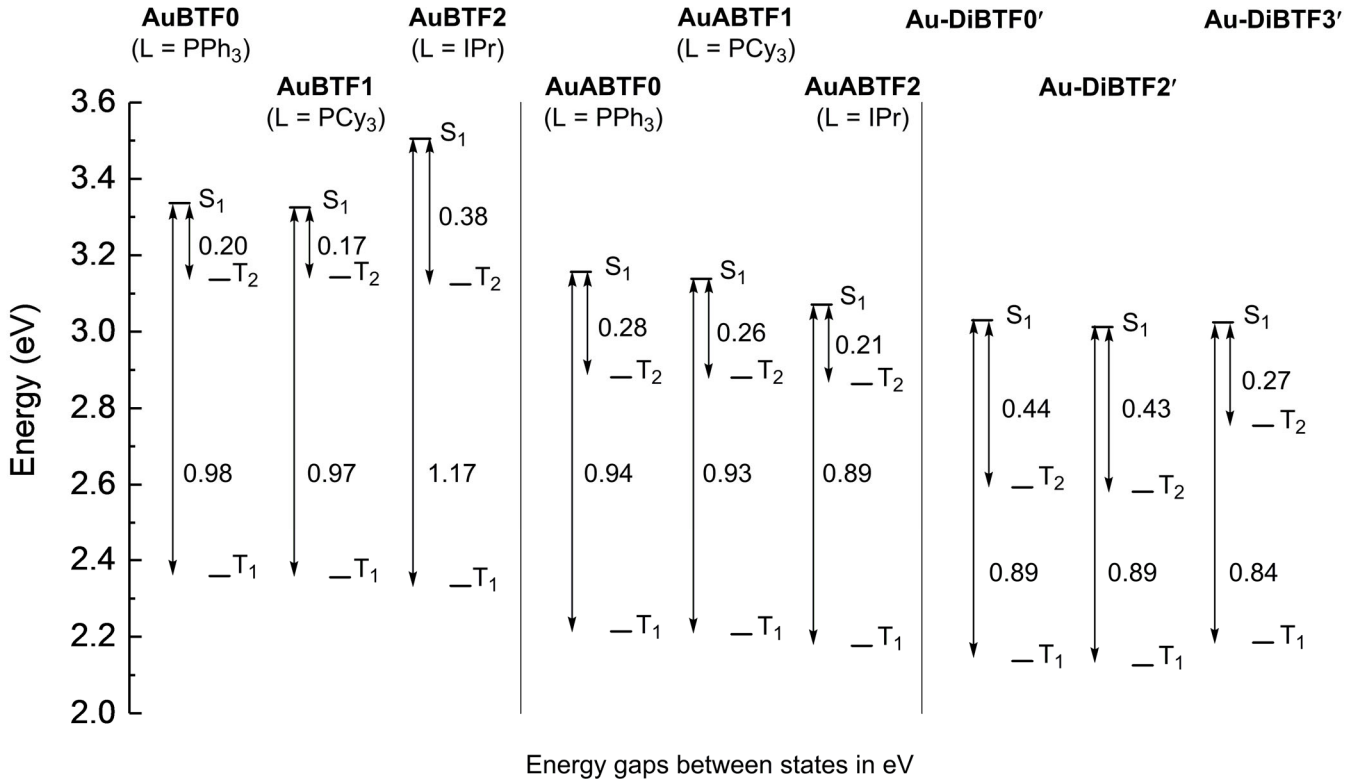

Figure 9. Time-dependent density-functional theory (TD-DFT) state plot for **Au-BTF(0-2), Au-ABTF(0-2), and (Au-DiBTF (0,2,3)'** showing S_1, T_2, and T_1 states. Energies are in electron volts (eV)

Energies of Franck-Condon singlet and triplet excited states were calculated with time-dependent density functional theory (TD-DFT). Figure 9 plots energies of the Franck-Condon excited states of **Au-ABTF(0-2)** as well as **Au-BTF(0-2)** and **Au-DiBTF(0,2,3).** Regarding the new compounds **Au-ABTF(0-2);** the carbene complex **(Au-ABTF2)** has the smallest energy gap (0.21 eV) between the first singlet (S_1) and nearest triplet excited state (T_2). **Au-ABTF0** and **Au-BTF1** have slightly larger gaps with similar values of 0.28 eV and 0.26 eV respectively. These calculations accord with experimental results where **Au-ABTF2** has a k_{isc} that is nearly twice that of either phosphine complex. **Au-ABTF2** also has the highest triplet state quantum yield. In every series of compounds (aryl, alkynyl, and di-gold), the complex that has the fastest intersystem crossing also displays the smallest computed S_1-T_2 energy gap (Figure 9).

Conclusions. Three new gold(I) alkynyl complexes of fluorene-benzothiazole substituted chromophores were synthesized and photophysically examined containing different ancillary ligands. Under freeze-pump-thaw deaerated conditions, all complexes exhibit dual luminescence at room temperature. Fluorescence lifetimes are on the order of hundreds of picoseconds with phosphorescent lifetimes on the order of hundreds of microseconds. Intersystem crossing and radiative decay are the dominant kinetic pathways in all three complexes. The radiative decay rates are nearly identical in **Au-ABTF(0-2)**. The rate of intersystem crossing is two times faster in the *N*-heterocyclic carbene complex, **Au-ABTF2**, compared with the phosphine containing complexes, **Au-ABTF0** and **Au-ABTF1**. Transient absorption experiments established extremely strong excited-state absorption for in both the singlet and triplet excited-states of **Au-ABTF(0-2)**. Power dependent transient absorption decays along with the observation of delayed fluorescence led to the determination of diffusion controlled triplet-triplet annihilation in solutions of **Au-ABTF(0-2)**. Both static and time-resolved density-functional theory calculations accord with the observed photophysical data, which suggest that the alkynyl linkage impedes intersystem crossing in comparison to σ-bonded gold(I)-aryl analogues. The HOMO and LUMO of all three complexes are localized on the alkynyl chromophore with small contributions from gold. TD-DFT calculations show that the phosphine complexes have slightly larger S_1- T_2 energy gaps (0.28 eV and 0.26 eV) compared to the carbene complex (0.21 eV). This result agrees with the larger k_{isc} and triplet-state yield of **Au-ABTF2** compared to **Au-ABTF(0-1)**. A comparison with our earlier (aryl)gold(I) analogues and di-gold(I) complexes of the BTF chromophore suggests design rules for tailoring the photophysical properties in this series of gold(I) chromophores. The aryl **Au-BTF** compounds exhibit an increase in fluorescence lifetime and quantum yield and a decrease in intersystem crossing efficiency when the ancillary ligand is changed from a phosphine to a carbene. The opposite effect occurs for (alkynyl)gold(I) analogues. With a change from phosphine- to carbene ligation, intersystem crossing is more efficient, with shorter lifetimes and smaller yields of fluorescence. Synthetically modifying the alkynyl linkage in **Au-DiBTF2** to a triazolyl in **Au-DiBTF3** results in a further decrease in fluorescence lifetime and quantum yield with more efficient intersystem crossing. Taken together, we have demonstrated that structure-property relationships in both mononuclear and binuclear gold(I) complexes can be altered through facile

synthetic tuning of either ancillary ligand, changing the nature of the gold-chromophore bond, or including multiple gold(I) centers. Synthesis, photophysics, and computational details of further gold(I) complexes with varying organic ancillary ligands and chromophores will be reported in due course in order to further bolster our understanding of structure property relationships in gold(I) chromophores.

References

1 M. C. Tang, C. H. Lee, M. Ng, Y. C. Wong, M. Y. Chan and V. W. W. Yam, Highly Emissive Fused Heterocyclic Alkynylgold(III) Complexes for Multiple Color Emission Spanning from Green to Red for Solution-Processable Organic Light-Emitting Devices, *Angew. Chemie - Int. Ed.*, 2018, **57**, 5463–5466.

2 M. C. Tang, M. Y. Leung, S. L. Lai, M. Ng, M. Y. Chan and V. Wing-Wah Yam, Realization of Thermally Stimulated Delayed Phosphorescence in Arylgold(III) Complexes and Efficient Gold(III) Based Blue-Emitting Organic Light-Emitting Devices, *J. Am. Chem. Soc.*, 2018, **140**, 13115–13124.

3 Y. Yuan, P. Gnanasekaran, Y. W. Chen, G. H. Lee, S. F. Ni, C. S. Lee and Y. Chi, Iridium(III) Complexes Bearing a Formal Tetradentate Coordination Chelate: Structural Properties and Phosphorescence Fine-Tuned by Ancillaries, *Inorg. Chem.*, 2019, **59**, 523–532.

4 Z. Hao, K. Zhang, P. Wang, X. Lu, Z. Lu, W. Zhu and Y. Liu, Deep Red Iridium(III) Complexes Based on Pyrene-Substituted Quinoxaline Ligands for Solution-Processed Phosphorescent Organic Light-Emitting Diodes, *Inorg. Chem.*, 2019, **59**, 332–342.

5 R. C. Evans, P. Douglas and C. J. Winscom, Coordination complexes exhibiting room-temperature phosphorescence: Evaluation of their suitability as triplet emitters in organic light emitting diodes, *Coord. Chem. Rev.*, 2006, **250**, 2093–2126.

6 G. M. Farinola and R. Ragni, Electroluminescent materials for white organic light emitting diodes, *Chem. Soc. Rev.*, 2011, **40**, 3467–3482.

7 M. E. Thompson, P. E. Burrows and S. R. Forrest, Electrophosphorescence in organic light emitting diodes, *Curr. Opin. Solid State Mater. Sci.*, 1999, **4**, 369–372.

8 M. C. Tang, C. H. Lee, S. L. Lai, M. Ng, M. Y. Chan and V. W. W. Yam, Versatile Design Strategy for Highly Luminescent Vacuum-Evaporable and Solution-Processable Tridentate Gold(III) Complexes with Monoaryl Auxiliary Ligands and Their Applications for Phosphorescent Organic Light Emitting Devices, *J. Am. Chem. Soc.*, 2017, **139**, 9341–9349.

9 P. T. Furuta, L. Deng, S. Garon, M. E. Thompson and J. M. J. Fréchet, Platinum-functionalized random copolymers for use in solution-processible, efficient, near-white organic light-emitting diodes, *J. Am. Chem. Soc.*, 2004, **126**, 15388–15389.

10 S. Lamansky, P. Djurovich, D. Murphy, F. Abdel-Razzaq, H. E. Lee, C. Adachi, P. E. Burrows, S. R. Forrest and M. E. Thompson, Highly phosphorescent bis-cyclometalated iridium complexes: Synthesis, photophysical characterization, and use in organic light emitting diodes, *J. Am. Chem. Soc.*, 2001, **123**, 4304–4312.

11 W. P. To, D. Zhou, G. S. M. Tong, G. Cheng, C. Yang and C. M. Che, Highly Luminescent Pincer Gold(III) Aryl Emitters: Thermally Activated Delayed Fluorescence and Solution-Processed OLEDs, *Angew. Chemie - Int. Ed.*, 2017, **56**, 14036–14041.

12 M. A. Baldo, D. F. O. an dY. You, A. Shoustikov, S. Sibley, M. E. Thompson and S. R. Forrest, Highly efficient phosphorescent emission from organic electroluminescent devices, *Nature*, 1998, **395**, 151.

13 C. Adachi, M. A. Baldo, M. E. Thompson and S. R. Forrest, Nearly 100% internal phosphorescence efficiency in an organic light emitting device, *J. Appl. Phys.*, 2001, **90**, 5048–5051.

14 J. Kalinowski, V. Fattori, M. Cocchi and J. A. G. Williams, Light-emitting devices based on organometallic platinum complexes as emitters, *Coord. Chem. Rev.*, 2011, **255**, 2401–2425.

15 Q. Zeng, F. Li, Z. Chen, K. Yang, Y. Liu, T. Guo, G.-G. Shan and Z.-M. Su, Rational Design of Efficient Organometallic Ir(III) Complexes for High-Performance Flexible Monochromatic and White Light-Emitting Electrochemical Cells, *ACS Appl. Mater. Interfaces*, 2020, **12**, 4649–4658.

16 M. Mydlak, C. Bizzarri, D. Hartmann, W. Sarfert, G. Schmid and L. De Cola, Positively charged iridium(lll) triazole derivatives as blue emitters for light-emitting electrochemical cells, *Adv. Funct. Mater.*, 2010, **20**, 1812–1820.

17 C. Ulbricht, B. Beyer, C. Friebe, A. Winter and U. S. Schubert, Recent developments in the application of phosphorescent iridium(III) complex systems, *Adv. Mater.*, 2009, **21**, 4418–4441.

18 H. C. Su, H. F. Chen, F. C. Fang, C. C. Liu, C. C. Wu, K. T. Wong, Y. H. Liu and S. M. Peng, Solid-state white light-emitting electrochemical cells using iridium-based cationic transition metal complexes, *J. Am. Chem. Soc.*, 2008, **130**, 3413–3419.

19 R. D. Costa, E. Ortí, H. J. Bolink, F. Monti, G. Accorsi and N. Armaroli, Luminescent ionic transition-metal complexes for light-emitting electrochemical cells, *Angew. Chemie - Int. Ed.*, 2012, **51**, 8178–8211.

20 R. Vestberg, R. Westlund, A. Eriksson, C. Lopes, M. Carlsson, B. Eliasson, E. Glimsdal, M. Lindgren and E. Malmström, Dendron decorated platinum(II) acetylides for optical power limiting, *Macromolecules*, 2006, **39**, 2238–2246.

21 N. J. Long, Organometallic Compounds for Nonlinear Optics—The Search for En-light-enment!, *Angew. Chemie Int. Ed. English*, 1995, **34**, 21–38.

22 M. J. Miller, A. G. Mott and B. P. Ketchel, General optical limiting requirements, *Nonlinear Opt. Liq. Power Limiting Imaging*, 2003, **3472**, 24.

23 S. R. Marder, B. Kippelen, A. K. Y. Jen and N. Peyghambarian, Design and synthesis of chromophores and polymers for electro-optic and photorefractive applications, *Nature*, 1997, **388**, 845–851.

24 G. J. Zhou and W. Y. Wong, Organometallic acetylides of PtII, AuI and Hg II as new generation optical power limiting materials, *Chem. Soc. Rev.*, 2011, **40**, 2541–2566.

25 G. S. He, L.-S. Tan, Q. Zheng and P. N. Prasad, Multiphoton Absorbing Materials: Molecular Designs, Characterizations, and Applications, *Chem. Rev.*, 2008, **108**, 1245–1330.

26 B. Liu, Z. Tian, F. Dang, J. Zhao, X. Yan, X. Xu, X. Yang, G. Zhou and Y. Wu, Photophysical and optical power limiting behaviors of Au(I) acetylides with diethynyl aromatic ligands showing different electronic features, *J. Organomet. Chem.*, 2016, **804**, 80–86.

27 P. B. Jacques Simon, Design of Molecular Materials: Supramolecular Engineering, *Wiley*, 2001, **15**, 197–199.

28 Y. Lin, C. Jiang, F. Hu, J. Yin, G. A. Yu and S. H. Liu, Synthesis, characterization, and properties of some bisacetylide and binuclear acetylide gold(I) compounds based on the photochromic dithienylethene unit, *Dye. Pigment.*, 2013, **99**, 995–1003.

29 K. T. Chan, G. S. M. Tong, W. P. To, C. Yang, L. Du, D. L. Phillips and C. M. Che, The interplay between fluorescence and phosphorescence with luminescent gold(i) and gold(iii) complexes bearing heterocyclic arylacetylide ligands, *Chem. Sci.*, 2017, **8**, 2352–2364.

30 S. Cekli, R. W. Winkel, E. Alarousu, O. F. Mohammed and K. S. Schanze, Triplet excited state properties in variable gap π-conjugated donor-Acceptor-donor chromophores, *Chem. Sci.*, 2016, **7**, 3621–3631.

31 S. Goswami, G. Wicks, A. Rebane and K. S. Schanze, Photophysics and non-linear absorption of Au(i) and Pt(ii) acetylide complexes of a thienyl-carbazole chromophore, *Dalt. Trans.*, 2014, **43**, 17721–17728.

32 S. Goswami, R. W. Winkel and K. S. Schanze, Photophysics and Nonlinear Absorption of Gold(I) and Platinum(II) Donor-Acceptor-Donor Chromophores, *Inorg. Chem.*, 2015, **54**, 10007–10014.

33 Q. Zhao, C. Huang and F. Li, Phosphorescent heavy-metal complexes for bioimaging, *Chem. Soc. Rev.*, 2011, **40**, 2508–2524.

34 H. Xiang, J. Cheng, X. Ma, X. Zhou and J. J. Chruma, *Near-infrared phosphorescence: Materials and applications*, 2013, vol. 42.

35 K. K. W. Lo, A. W. T. Choi and W. H. T. Law, Applications of luminescent inorganic and organometallic transition metal complexes as biomolecular and cellular probes, *Dalt. Trans.*, 2012, **41**, 6021–6047.

36 D. L. Ma, H. Z. He, K. H. Leung, D. S. H. Chan and C. H. Leung, Bioactive luminescent transition-metal complexes for biomedical applications, *Angew. Chemie - Int. Ed.*, 2013, **52**, 7666–7682.

37 K. Li, G. S. Ming Tong, Q. Wan, G. Cheng, W. Y. Tong, W. H. Ang, W. L. Kwong and C. M. Che, Highly phosphorescent platinum(ii) emitters: photophysics, materials and biological applications, *Chem. Sci.*, 2016, **7**, 1653–1673.

38 X. Z. Shu, M. Zhang, Y. He, H. Frei and F. D. Toste, Dual visible light photoredox and gold-catalyzed arylative ring expansion, *J. Am. Chem. Soc.*, 2014, **136**, 5844–5847.

39 O. Reiser, G. Kachkovskyi, V. Kais, P. Kohls, S. Paria, M. Pirtsch, D. Rackl and H. Seo, Walter de Gruyter GmbH, 2013, p. 139.

40 M. H. Shaw, J. Twilton and D. W. C. MacMillan, Photoredox Catalysis in Organic Chemistry, *J. Org. Chem.*, 2016, **81**, 6898–6926.

41 Y. You and W. Nam, Photofunctional triplet excited states of cyclometalated Ir(III) complexes: Beyond electroluminescence, *Chem. Soc. Rev.*, 2012, **41**, 7061–7084.

42 C. K. Prier, D. A. Rankic and D. W. C. MacMillan, Visible light photoredox catalysis with transition metal complexes: Applications in organic synthesis, *Chem. Rev.*, 2013, **113**, 5322–5363.

43 M. D. Levin, S. Kim and F. D. Toste, Photoredox catalysis unlocks single-electron elementary steps in transition metal catalyzed cross-coupling, *ACS Cent. Sci.*, 2016, **2**, 293–301.

44 M. N. Hopkinson, A. Tlahuext-Aca and F. Glorius, Merging Visible Light Photoredox and Gold Catalysis, *Acc. Chem. Res.*, 2016, **49**, 2261–2272.

45 J. Zhao, W. Wu, J. Sun and S. Guo, Triplet photosensitizers: From molecular design to applications, *Chem. Soc. Rev.*, 2013, **42**, 5323–5351.

46 J. F. Longevial, K. El Cheikh, D. Aggad, A. Lebrun, A. van der Lee, F. Tielens, S. Clément, A. Morère, M. Garcia, M. Gary-Bobo and S. Richeter, Porphyrins Conjugated with Peripheral Thiolato Gold(I) Complexes for Enhanced Photodynamic Therapy, *Chem. - A Eur. J.*, 2017, **23**, 14017–14026.

47 L. Zhou, X. Ge, J. Liu, J. Zhou, S. Wei, F. Li and J. Shen, Internal heavy atom effect of Au(III) and Pt(IV) on hypocrellin A for enhanced in vitro photodynamic therapy of cancer, *Bioorganic Med. Chem. Lett.*, 2013, **23**, 5317–5324.

48 E. Baggaley, J. A. Weinstein and J. A. G. Williams, Lighting the way to see inside the live cell with luminescent transition metal complexes, *Coord. Chem. Rev.*, 2012, **256**, 1762–1785.

49 L. K. McKenzie, H. E. Bryant and J. A. Weinstein, Transition metal complexes as photosensitisers in one- and two-photon photodynamic therapy, *Coord. Chem. Rev.*, 2019, **379**, 2–29.

50 X. Jiang, N. Zhu, D. Zhao and Y. Ma, New cyclometalated transition-metal based photosensitizers for singlet oxygen generation and photodynamic therapy, *Sci. China Chem.*, 2016, **59**, 40–52.

51 D. V. Partyka, A. J. Esswein, M. Zeller, A. D. Hunter and T. G. Gray, Gold(I) pyrenyls: Excited-state consequences of carbon-gold bond formation, *Organometallics*, 2007, **26**, 3279–3282.

52 L. Gao, M. A. Peay, D. V. Partyka, J. B. Updegraff, T. S. Teets, A. J. Esswein, M. Zeller, A. D. Hunter and T. G. Gray, Mono- and di-gold(I) naphthalenes and pyrenes: Syntheses, crystal structures, and photophysics, *Organometallics*, 2009, **28**, 5669–5681.

53 Y. Dong, J. Zhang, A. Li, J. Gong, B. He, S. Xu, J. Yin, S. H. Liu and B. Z. Tang, Structure-tuned and thermodynamically controlled mechanochromic self-recovery of AIE-active Au(i) complexes , *J. Mater. Chem. C*, 2020, 894–899.

54 I. D. Strelnik, V. V. Sizov, V. V. Gurzhiy, A. S. Melnikov, I. E. Kolesnikov, E. I. Musina, A. A. Karasik and E. V. Grachova, Binuclear Gold(I) Phosphine Alkynyl Complexes Templated on a Flexible Cyclic Phosphine Ligand: Synthesis and Some Features of Solid-State Luminescence, *Inorg. Chem.*, 2019, **59**, 244–253.

55 T. Seki, K. Kashiyama and H. Ito, Luminescent mechanochromism of gold N -heterocyclic carbene complexes with hypso- and bathochromic spectral shifts, *Dalt. Trans.*, 2019, **48**, 7105–7109.

56 N. M. W. Wu, M. Ng and V. W. W. Yam, Photochromic Benzo[b]phosphole Alkynylgold(I) Complexes with Mechanochromic Property to Serve as Multistimuli-Responsive Materials, *Angew. Chemie - Int. Ed.*, 2019, **58**, 3027–3031.

57 V. Fernández-Moreira, C. Val-Campillo, I. Ospino, R. P. Herrera, I. Marzo, A. Laguna and M. C. Gimeno, Bioactive and luminescent indole and isatin based gold(i) derivatives, *Dalt. Trans.*, 2019, **48**, 3098–3108.

58 E. Y. H. Hong and V. W. W. Yam, Triindole-tris-alkynyl-bridged trinuclear gold(I) complexes for cooperative supramolecular self-assembly and small-molecule solution-processable resistive memories, *ACS Appl. Mater. Interfaces*, 2017, **9**, 2616–2624.

59 M. C. Blanco, J. Cámara, V. Fernández-Moreira, A. Laguna and M. C. Gimeno, Gold(I), Phosphanes, and Alkynyls: The Perfect Allies in the Search for Luminescent Compounds, *Eur. J. Inorg. Chem.*, 2018, **2018**, 2762–2767.

60 J. J. González, E. Ortega, M. Rothemund, M. Gold, C. Vicente, C. De Haro, D. Bautista, R. Schobert and J. Ruiz, Luminescent Gold(I) Complexes of 1-Pyridyl-3-anthracenylchalcone Inducing Apoptosis in Colon Carcinoma Cells and Antivascular Effects, *Inorg. Chem.*, 2019, **58**, 12954–12963.

61 M. Głodek, S. Pawlędzio, A. Makal and D. Plażuk, The Impact of Crystal Packing and Aurophilic Interactions on the Luminescence Properties in Polymorphs and Solvate of Aroylacetylide–Gold(I) Complexes, *Chem. - A Eur. J.*, 2019, **25**, 13131–13145.

62 K. T. Chan, G. S. M. Tong, W. P. To, C. Yang, L. Du, D. L. Phillips and C. M. Che, The interplay between fluorescence and phosphorescence with luminescent gold(i) and gold(iii) complexes bearing heterocyclic arylacetylide ligands, *Chem. Sci.*, 2017, **8**, 2352–2364.

63 C. C. Beto, C. J. Zeman, Y. Yang, J. D. Bullock, E. D. Holt, A. Q. Kane, T. A. Makal, X. Yang, I. Ghiviriga, K. S. Schanze and A. S. Veige, An Application Exploiting Aurophilic Bonding and iClick to Produce White Light Emitting Materials, , DOI:10.1021/acs.inorgchem.9b03195.

64 K. T. Chan, G. S. M. Tong, W. P. To, C. Yang, L. Du, D. L. Phillips and C. M. Che, The interplay between fluorescence and phosphorescence with luminescent gold(i) and gold(iii) complexes bearing heterocyclic arylacetylide ligands, *Chem. Sci.*, 2017, **8**, 2352–2364.

65 G. S. Ming Tong, K. T. Chan, X. Chang and C. M. Che, Theoretical studies on the photophysical properties of luminescent pincer gold(III) arylacetylide complexes: The role of π-conjugation at the C-deprotonated [CΛNΛC] ligand, *Chem. Sci.*, 2015, **6**, 3026–3037.

66 R. A. Vogt, M. A. Peay, T. G. Gray and C. E. Crespo-Hernández, Excited-state dynamics of (Organophosphine)gold(I) pyrenyl isomers, *J. Phys. Chem. Lett.*, 2010, **1**, 1205–1211.

67 L. Gao, D. V. Partyka, J. B. Updegraff, N. Deligonul and T. G. Gray, Synthesis, structures, and excited-state geometries of alkynylgold(I) complexes, *Eur. J. Inorg. Chem.*, 2009, **2009**, 2711–2719.

68 D. V. Partyka, L. Gao, T. S. Teets, J. B. Updegraff, N. Deligonul and T. G. Gray, Copper-catalyzed huisgen [3 + 2] cycloaddition of gold(I) alkynyls with benzyl azide. Syntheses, structures, and optical properties, *Organometallics*, 2009, **28**, 6171–6182.

69 L. Gao, M. A. Peay, D. V. Partyka, J. B. Updegraff, T. S. Teets, A. J. Esswein, M. Zeller, A. D. Hunter and T. G. Gray, Mono- and di-gold(I) naphthalenes and pyrenes: Syntheses, crystal structures, and photophysics, *Organometallics*, 2009, **28**, 5669–5681.

70 J. J. Mihaly, D. J. Stewart, T. A. Grusenmeyer, A. T. Phillips, J. E. Haley, M. Zeller and T. G. Gray, Photophysical properties of organogold(i) complexes bearing a benzothiazole-2,7-fluorenyl moiety: Selection of ancillary ligand influences white light emission, *Dalt. Trans.*, 2019, **48**, 15917–15927.

71 J. J. Mihaly, A. T. Phillips, J. T. Malloy, Z. M. Marsh, M. Zeller, J. E. Haley, K. De La Harpe, T. A. Grusenmeyer and T. G. Gray, Synthesis and Photophysical Properties of Laterally Asymmetric Digold(I) Alkynyls and Triazolyl: Ancillary Ligand and Organic Functionality Dictate Excited-State Dynamics, *Organometallics*, 2020, **39**, 489–494.

72 J. E. Rogers, J. E. Slagle, D. M. Krein, A. R. Burke, B. C. Hall, A. Fratini, D. G. McLean, P. A. Fleitz, T. M. Cooper, M. Drobizhev, N. S. Makarov, A. Rebane, K. Y. Kim, R. Farley and K. S. Schanze, Platinum acetylide two-photon chromophores, *Inorg. Chem.*, 2007, **46**, 6483–6494.

73 D. V. Partyka, J. B. Updegraff, M. Zeller, A. D. Hunter and T. G. Gray, Carbon-gold bond formation through [3 + 2] cycloaddition reactions of gold(I) azides and terminal alkynes, *Organometallics*, 2007, **26**, 183–186.

74 J. E. Rogers, J. E. Slagle, D. M. Krein, A. R. Burke, B. C. Hall, A. Fratini, D. G. McLean, P. A. Fleitz, T. M. Cooper, M. Drobizhev, N. S. Makarov, A. Rebane, K. Y. Kim, R. Farley and K. S. Schanze, Platinum acetylide two-photon chromophores, *Inorg. Chem.*, 2007, **46**, 6483–6494.

75 S. Goswami, G. Wicks, A. Rebane and K. S. Schanze, Photophysics and non-linear absorption of Au(i) and Pt(ii) acetylide complexes of a thienyl-carbazole chromophore, *Dalt. Trans.*, 2014, **43**, 17721–17728.

76 S. Goswami, R. W. Winkel and K. S. Schanze, Photophysics and Nonlinear Absorption of Gold(I) and Platinum(II) Donor-Acceptor-Donor Chromophores, *Inorg. Chem.*, 2015, **54**, 10007–10014.

77 S. Goswami, G. Wicks, A. Rebane and K. S. Schanze, Photophysics and non-linear absorption of Au(i) and Pt(ii) acetylide complexes of a thienyl-carbazole chromophore, *Dalt. Trans.*, 2014, **43**, 17721–17728.

78 Y. C. Chang, K. C. Tang, H. A. Pan, S. H. Liu, I. O. Koshevoy, A. J. Karttunen, W. Y. Hung, M. H. Cheng and P. T. Chou, Harnessing fluorescence versus phosphorescence branching ratio in (Phenyl) n -bridged (n = 0-5) bimetallic Au(I) complexes, *J. Phys. Chem. C*, 2013, **117**, 9623–9632.

79 T. N. Singh-Rachford and F. N. Castellano, Photon upconversion based on sensitized triplet–triplet annihilation, *Coord. Chem. Rev.*, 2010, **254**, 2560–2573.

80 Montalti, A. Credi, L. Prodi and M. Teresa Gandolfi, *Handbook of Photochemistry, Third Edition*, CRC Press, 3rd Editio., 2006.

Acknowledgment. This work is supported by the Air Force Office of Scientific Research, contract FA9550-18-1-0247 to T. G. G. All AFRL affiliated authors recognize the Air Force Office of Scientific Research under AFOSR Award 9550-19-1-18RX056 and the Air Force Research Laboratory/RXAP contract FA8650-16-D-5402-0001. NSF is acknowledged through the Major Research Instrumentation Program under Grant No. CHE 1625543 to M. Z. (funding for the single crystal X-ray diffractometer).

Competing Interests. CWRU has filed for provisional patent protection of **Au-ABTF0-2.**

Author Contributions

‡ Joseph J. Mihaly and Alexis T. Phillips contributed equally.

ORCID NUMBERS

J. J. Mihaly: 0000-0002-2259-0713

D. J. Stewart: 0000-0003-3246-3723

T. G. Gray: 0000-0003-1756-8877

T. A. Grusenmeyer: 0000-0002-1842-056X

J. E. Haley: 0000-0001-5329-8291

A.T. Phillips: 0000-0003-4321-1409J.E. Haley: 0000-0001-5329-8291

C. L. McCleese: 0000-002-2114-8392

Electronic Supplementary Information (ESI) Available: Materials and experimental methods, synthetic details for **AuBTF0–2**, ^{1}H and ^{31}P NMR, mass spectrometry, elemental analysis, fluorescence and phosphorescence lifetime fits, fluorescence and phosphorescence quantum yield data, singlet oxygen phosphorescence quantum yield data, delayed fluorescence as a function of laser power, triplet-triplet annihilation fitting, data used to calculate excited-state extinction coefficients, ultrafast transient absorption kinetic fit data, a summary of the calculated electronic

transitions obtained from TD-DFT calculations for **AuBTF1** and **AuBTF2** and the details for X-ray crystallography data collection, work-up and experimental details for **AuBTF0** -**AuBTF2** are all included in the Supplementary Information.

Complete crystallographic data, in CIF format, have been deposited with the Cambridge Crystallographic Data Centre. CCDC 1917590-1917592 contains the supplementary crystallographic data for this paper. These data can be obtained free of charge from The Cambridge Crystallographic Data Centre via www.ccdc.cam.ac.uk/data_request/cif.

TOC Entry

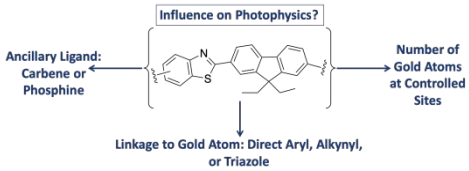
Influence on Photophysics?
Ancillary Ligand: Carbene or Phosphine
Number of Gold Atoms at Controlled Sites
Linkage to Gold Atom: Direct Aryl, Alkynyl, or Triazole
N
S